**Main Manuscript for**

# Diffusion power spectra as a window into dynamic materials architecture

Sophia N. Fricke[a,*], Mia Salgado[a], Shira Haber[b], Mutian Hua[b], Jeremy Demarteau[c], Ah-Young Song [a,b], Brett A. Helms[b,c], Jeffrey A. Reimer[a,b,*]


[a] Department of Chemical and Biomolecular Engineering, University of California, Berkeley, Berkeley, CA 94720, USA

[b] Materials Sciences Division, Lawrence Berkeley National Laboratory, Berkeley, CA 94720, USA

[c] Molecular Foundry, Lawrence Berkeley National Laboratory, Berkeley, CA 94720, USA


[*] Corresponding Authors, **Email:** snfricke@berkeley.edu, reimer@berkeley.edu

**This PDF file includes:**

> Main Text
> Figures 1 to 6

**Author contributions:** S.N.F. designed, performed, and analyzed research and wrote the paper, M.S. performed research and analyzed research, S.H. performed and analyzed research, M.H. initially observed the anion effect on PDK hydrolysis and synthesized materials, J.D. synthesized materials, A.S. performed research, B.A.H. and J.A.R. designed and directed the research and edited the paper.

**Competing Interest Statement:** The authors declare the following competing interests: B.A.H. is an inventor on the US provisional patent application 62/587,148 submitted by Lawrence Berkeley National Laboratory that covers PDKs, as well as aspects of their use and recovery. B.A.H. and J.D. are inventors on the US provisional patent application 63/390,962 submitted by Lawrence Berkeley National Laboratory that covers biorenewable PDKs, as well as aspects of their use and recovery. B.A.H. has a financial interest in Cyklos Materials and Sepion Technologies. The remaining authors declare no competing interests.

**Abstract**

Understanding molecular dynamics in heterogeneous environments is a foundational step in tuning macromolecular reactivity. This is especially important in the chemical recycling of commodity and specialty polymers, which is often undertaken in aqueous media using molecular or enzymatic catalysts. Yet, it remains a challenge study dynamic materials architectures without accurate discernment of the behavior of water in confining media to capture the complexity of the operative transport processes. Here, we develop experimental and analytical methodologies describing the complete set of diffusive eigenmodes that exist within time-varying, non-Euclidean boundary conditions—a situation commonly found in the reactive deconstruction of polymers. Diffusion power spectra, as discerned by an NMR-based method, yield frequency-domain velocity autocorrelation functions that are analyzed in the context of physical models parameterized with fractal mathematics. The results connect time-evolving local motion in polymers to chemical reactivity during acid-catalyzed deconstruction of elastomers. The fundamental understanding provided herein offers practical tools for engineering materials with tailored properties and behaviors, with particular attention to the design of reactive polymers that advance circular materials economies and sustainable chemistry practices.

**Keywords:** NMR, restricted diffusion, porous media, polymers, velocity autocorrelation spectra

**Introduction**

Advanced polymer networks not only offer custom material properties, but can also change or degrade in time. Understanding the dynamics of these networks, from molecular to macroscopic scales, is crucial to tracking these changes throughout one or more cycles of use. Such insights would facilitate a shift from a linear to a circular materials economy, addressing the urgent need for more efficient and effective chemical recycling of polymers.(*1–3*) Despite the ubiquity of polymers, their complex architecture presents challenges for characterization, modeling, and design when their systematic descriptions deviate from classical models defined within Euclidean frameworks. This departure from Euclidean geometry in nano- and microporous media influences the thermal motion of confined molecules.(*4, 5*) The nature of confinement, such as in an elastomer undergoing chemical transformation, has a profound influence on the motion of trapped molecules, serving as time-varying boundary conditions for diffusion. In the absence of confinement, molecular motion corresponds to plane wave eigenmodes, with momenta states given by $\hbar k$. When a molecule experiences confinement, the boundary conditions restrict its allowed states due to the requirement of zero probability at the boundaries.(*6*) When the boundaries exhibit surface roughness and irregularities that may be approximated with fractional dimensionality, the diffusion equation must be solved with the constraints of these complex boundary conditions.(*7, 8*) This approach is necessary to quantify essential yet underexplored aspects of polymer deconstruction to reusable monomers.

The fractal nature of a heterogeneous network boundary (e.g., pore walls) alters Brownian motion of proximal molecules.(*9–11*) Namely, molecular movement exhibits non-random modes that deviate from a traditional Markovian description. The prolonged memory that arises from confinement and influences extended motional coherence is manifested in the velocity autocorrelation function as a time tail that extends beyond a Gaussian decay.(*12, 13*) This non-Brownian contribution to molecular motion is observable in a diffusion power spectrum, i.e., the spectral density of the velocity autocorrelation function.(*14–16*) It is convenient to measure these diffusion spectra with nuclear magnetic resonance (NMR) via modulated gradient spin echo (MGSE) trains.(*17*) Benefits of the MGSE NMR approach include detection of entire sample volumes, versus simply surfaces as with dynamic light scattering and related approaches, thereby shedding light on the bulk evolving internal pore structures and connectivity. In particular, the use of low field, unilateral magnets to accomplish the NMR measurement enables observation of a wide variety of sample geometries, and readily captures the effects of both volume heterogeneity and surface complexity. Moreover, the time- and length-scales accessible via frequency-filtered

MGSE trains are some of the widest of the available experimental techniques, readily spanning frequencies of molecular motion from 0-10,000 Hz. Yet, MGSE NMR has not been widely applied to the dynamic materials architecture in polymers or nano- and microporous systems, which manifest during polymer deconstruction and chemical recycling processes.

Here, we report a facile implementation of MGSE NMR, options for interpretation of the rich data these experiments afford, as well as theoretical validation of this approach that is consistent with a nonlinear derivation of molecular self-diffusion. Diffusion power spectra obtained from these experiments are presented as an efficient experimental means of observing molecular dynamics across broad length- and time-scales in the complex and evolving media associated with polymer deconstruction. We show that these diffusion spectra report porous network confinement with a high degree of sensitivity and resolution for a series of elastomers varying in their dynamic materials architectures on the basis of both chemical crosslinks and entanglement.(*18*)

**Results**

Leveraging the complexities of polymer transport and diffusion presents a unique opportunity for designing circular processes with enhanced efficiency and sustainability. The interplay of polymer dynamics, including factors such as chain length, network entanglement, and interactions with surrounding environments, offers a rich landscape for tailoring material transport properties. The inset in Fig. 1A depicts a crosslinked elastomer network undergoing acidolytic transformation, a process mediated by diffusive transport of solvated protons through a heterogeneous medium. From the MGSE pulse sequence shown diagrammatically in Fig. 1B, the exemplary data in Fig. 1C demonstrate that the normalized echo amplitudes decay from diffusive signal attenuation as a function of the number of echoes, $N_{echoes}$; relaxation does not contribute to this attenuation because all echo trains are recorded with the same fixed total time, $T_{total}$. The energy level diagram in Fig. 1D contrasts the density of states available to stiff versus flexible polymer chains, where increasing polymer flexibility, entanglement, and crosslink density serve to broaden the continuum of states available to a polymer system. Correspondingly, the dynamic regimes accessed by a polymer system may be described by a diffusion spectrum, shown in Fig. 1E, which can be interpreted through changes in its power law scaling from low to high frequencies as progression from free diffusion, to reptation, Rouse, and finally to sub-segmental motion.(*19*)

4

### *Reaction kinetics are scale-variant in heterogeneous systems*

Chemical reaction kinetics are fundamentally influenced by the scale of a reaction and the surface areas upon or within which reactants interact.([20]) At the macroscopic level, large-scale reactions may exhibit kinetic behaviors that diverge from classical predictions based solely on consideration of micro- or nano- scale chemistry with homogeneously distributed reactants and products. In the classically ideal case, the increased effective surface area in small-scale reactions enhances the frequency of molecular collisions, facilitating more rapid reaction rates. However, discrepancies arise in the translation to macroscopic regimes where heterogeneous reactions are frequently observed, and reactants must interact across or diffuse through interfaces.([4–6, 12, 21, 22]) Additionally, surface-area dependencies become crucial when dealing with catalysts or porous materials, as the active sites available for reaction initiation are directly related to the exposed surface.([20]) Understanding the relationship between reaction kinetics, scale variance, and surface area dependence is vital for designing efficient chemical processes and optimizing reaction conditions, and leveraging the dynamic interplay between molecular entities at different scales.

Figure 2 illustrates the effect of surface area variation on the instantaneous rate coefficient for a depolymerization reaction, and the calculated Hurst exponent ($h$) and corresponding fractal dimension, which is an indicator of the degree of anisotropy present in the system through surface complexity and volume heterogeneity. Through this comparison of chemically identical crosslinked polydiketoenamine (PDK-T5000) elastomers deconstructing in the same reaction medium, prepared in cylindrical geometries of 5 mm in height but with diameters ranging from 4–8 mm, it is evident that the depolymerization rate scales inversely with the sample size.

Moreover, regimes of sub-, Brownian, and super-diffusion are observed in Fig. 2B, corresponding to $h < 0.5$, $h = 0.5$, and $h > 0.5$, respectively.([11]) A shift from predominantly superdiffusion at early times to subdiffusion at late times represents the initial prevalence of active transport via polymer swelling being gradually replaced by isotropic yet restricted molecular movement. This interpretation reflects a spatial average resulting from all the modes of diffusion present simultaneously within the sample. The time-variation of $h$ may be understood as the rate of reaction deceleration, or the "jerk" – a vector quantity that corresponds to the third derivative of the position of the reaction front over time.([23]) Nonzero jerk may be understood as the minimum requirement for chaotic behavior in a system, and successive time-derivatives (termed snap,

5

crackle, and pop) may be used to linearize the behavior of the chemical wavefront and to model deceleration from the maximum, classically predicted speed.(*24*)

To better understand the influence of restricted diffusion, we consider the contributions of different frequencies of molecular motion to the superposed modes of diffusion that are collectively detected by measuring power spectra via MGSE NMR experiments.(*15*) In an MGSE experiment, a magnetization grating is selectively increased by varying the frequency of echo train $\pi$ pulses within a fixed total time and constant linear magnetic field gradient. This creates a low-pass filter for spin phase coherences corresponding to molecules within the entire volume of the sample that move at similar frequencies; typically, a superposition of these contributions is detected altogether. By resolving individual contributions across a frequency spectrum, it is possible to understand deeper aspects relating to both the structure and dynamics of a heterogeneous polymer system, and how they are interrelated. The frequency-dependent diffusion coefficient, $D(\omega)$, may be understood(*16*) as the transport property associated with the velocity autocorrelation function

$$D(\omega) = \frac{1}{3}\int_0^\infty e^{-i\omega t}\langle v(0) \cdot v(t)\rangle dt \tag{1}$$

where $v(t)$ represents the time-dependent velocity, and the scaling by $\frac{1}{3}$ is a dimensional factor corresponding to the magnetic field gradient. In general, the Green–Kubo relations provide a template to obtain the frequency dependence of any other transport property similarly associated with a spatial or temporal autocorrelation function.(*25*) This is achieved formulaically by relating a macroscopic transport coefficient to the Fourier transform of a correlation function of a microscopic variable. We now consider three cases that may collectively shed light on deconstructing polymer systems.

### Diffusion power spectra reflect water confinement and polymer network architecture

First, we study the confined modes of water diffusion within various swelled elastomer networks without the temporal influence of chemical reaction (Fig. 3). This is an indirect measurement using the abundant proton signal from water as a probe of confining material architecture. It is evident in Fig. 3A that increased high-frequency modes of diffusion are available

6

to water in confined environments provided by network polymers compared to unrestricted water, oil, and a micellar gel Pluronic F-127. Thus, observation of increased aqueous diffusivity probed at frequencies of 5–10 kHz or greater reports degree of confinement in surrounding network architecture. The degree of this increase may be conveniently expressed by plotting the scaling power of $D(\nu)$, from which $h(\nu)$ is readily calculated from an expression for fractional Brownian motion unrestricted to linear scaling in time as

$$D(t) = \alpha t^{\alpha-1} D \qquad (2)$$

where the constant $\alpha$ is twice the Hurst exponent.(11)

By plotting normalized frequency-dependent diffusivities of different systems relative to $D(\nu)$ for water (Fig. 3B) and oil (Fig. 3C), it is possible to isolate the specific changes in the diffusion power spectra that relate to confinement and the dipolar coupling provided by an organic alkane backbone, respectively. From comparison to the diffusion spectrum for free water in Fig. 3B, it is apparent that the majority of changes in diffusion spectra for systems with some degree of confinement are manifested in the low-frequency regime of 0–5 kHz. This corresponds with the frequency range of molecular motions commonly attributed to translational dynamics for small molecules and reptation dynamics for large molecules, depicted in Fig. 1D and 1E.(19, 26) From the diffusion spectra scaling powers shown in Fig. 3D, it is possible to calculate the frequency-dependence of the Hurst exponents, $h(\nu)$, as described and simulated in ref. (11), and the relative change in $h(\nu)$ as compared to that of oil (Figs. 3E and 3F, respectively). Notably, water confined in the smallest network polymer, PDK-T403 (plotted in gold), presents the largest $h$ at high frequencies (6–8 kHz), followed by water confined in the polymeric anion exchange resin, Lewatit® VP OC 1065(27) (plotted in purple). In contrast, these two systems possess the smallest values of $h$ at low frequencies from approximately 2–4 kHz. Altogether, these trends appear to result from a higher degree of entanglement and therefore tighter confinement of water in these systems, which manifests in enhanced high-frequency correlated aqueous motion, and suppressed low-frequency, long-range translational motion.

Next, we immerse the same series of elastomer networks with $D_2O$ to selectively study only the slower modes of motion of the polymer networks themselves. As illustrated in Fig. 4A, the increase in diffusivity of network protons appears to correspond to increasing network size from the micellar gel Pluronic F-127, to PDK-T403, to Lewatit, to PDK-T3000 and PDK-T5000,

7

which are statistically indistinguishable in this regard. Moreover, increased diffusivity probed at frequencies of 5–10 kHz or more may indicate detection of higher order vibrational modes of polymer stretching, which may be described by Rouse and Zimm models of polymer dynamics(*19, 26*), conceptually illustrated in Fig. 1E, and quantified via calculation and analysis of $h(v)$.

Analysis of normalized frequency-dependent diffusivities of different systems relative to $D(v)$ for oil (Fig. 4B) and water (Fig. 4C) highlights explicit changes in the diffusion power spectra that represent departures from signatures related to the dipolar coupling provided by an organic alkane backbone and free diffusion of unconfined water, respectively. From comparison to the diffusion spectrum for free water in Fig. 4C, it is apparent that high-frequency modes of diffusion are most amplified for systems with low crosslink density. This corresponds to the frequency range of molecular motions commonly attributed to vibrational dynamics.(*26*) One possible interpretation of this result is that the smaller network polymers may be too tightly entangled to develop higher modes of vibration, whereas larger network polymers with relatively lower crosslink density may support a higher harmonic range of vibrational movement.

From the diffusion spectra scaling powers shown in Fig. 4D, it is possible to calculate(*11*) the frequency-dependence of the Hurst exponents, $h(v)$, and the relative change in $h(v)$ as compared to that of oil (Figs. 4E and 4F, respectively). Notably, the smallest network polymer, PDK-T403 (plotted in gold), presents the largest $h$ at high frequencies (6–8 kHz), followed by Lewatit (plotted in purple). In contrast, these two systems possess the smallest values of $h$ at low frequencies from approximately 2–4 kHz. The apparent divergence from this trend below 2 kHz may result from differences in the overlap between free diffusion and reptation-type movement of Lewatit, an anion-exchange resin, and PDK elastomers. Altogether, these trends appear to result from a higher degree of entanglement in these systems, which manifests in enhanced high-frequency vibrational motion, and suppressed low-frequency, long-range translational motion (most apparent for PDK-T403), consistent with the results suggested in parallel from study of confined aqueous diffusion in these systems in Fig. 3. This observation is consistent with the results of previous studies that suggested one effect of crosslinking is to lock a polymer network into a non-equilibrium state as compared to the same network prior to the introduction of crosslinks.(*28, 29*) By extension, it may be surmised that networks with higher crosslink density will occupy states farther from equilibrium than those with low crosslink density, which manifests as more extreme scaling behavior.(*30, 31*)

***A fractal model links structural and kinetic insights from time-resolved diffusion power spectra***

Next, we record time-resolved MGSEs in *operando* during polymer deconstruction for PDK-T403 in HBr, HCl, and $H_2SO_4$. The acids respectively donate chaotropic, order-neutral, and kosmotropic anions to the reaction medium, modulating the solvation shells and thereby varying the effective surface areas and pore volumes available for reaction (Figure 5). Calculation of $h(v)$ from $D(v)$ allows estimation of the time- and frequency-resolved rate coefficients, $k(v,t)$, as

$$k(t) = k(0)t^{-h}. \tag{3}$$

This formula has been applied previously to develop rate laws with non-integer molecularity and time-dependent rate coefficients(*32, 33*), and utilizes a power law framework that has been well-established in other areas of fractal mathematics.(*8, 34–37*)

Numerical integration of the Hurst exponent yields a prediction of frequency- and time-dependent rate coefficients, provided that the reaction studied proceeds in the slow, diffusion-mediated limit. Observation of the system in this limit allows the assumption that the kinetic and thermodynamic effects governing the process are operative in analogous timescales. An analytical expression can be developed via Laplace transformation of the Eq. (3), yielding the solution for $k$ in terms of the Laplace frequency, $s$, as a power law product with a gamma function

$$k(s) \cong s^{h-1}\Gamma(1-h). \tag{4}$$

For the cases considered in Fig. 5, while relative rates vary from fastest (HBr; green panel backdrop) to slowest ($H_2SO_4$; red panel backdrop), there is a trend of decreasing high-frequency modes of diffusion as the reaction progresses from 0 h (pale blue) to 48 h (dark blue), at which time even the slowest deconstructing system in $H_2SO_4$ had achieved complete depolymerization. This trend is consistent with diminishing crosslink density as the polymer network breaks apart, which serves to decrease the network confinement of trapped water. To explain this, we note that the decreased diffusive attenuation (i.e., higher values of $D(v)$ in Fig. 5A–C) arises from enhanced spin coherence, evident in diffusion power spectra with scaling greater than Rouse-type $\propto v^{3/4}$.

9

In the early stages of reaction, this is indicative of non-Brownian movement of confined water. As depolymerization progresses and the network breaks apart, the water and released monomer molecules become less correlated in their movement until free tumbling and rotation in solution are the predominant mechanisms of molecular motion.(*38*) As the aqueous reaction medium gains concentration of released monomer, the free tumbling of aqueous molecules becomes more hindered, resulting in increased viscosity and a corresponding decrease in the Hurst exponent as reaction time progresses, shown in Fig. 5D–F. Whereas there is not a hugely discernible change in rate coefficient over time for the fastest-deconstructing system shown in Fig. 5G, as the reaction medium becomes more kosmotropic (Fig. 5H–I), the rate coefficient shows a marked decrease over time for the low- and high-frequency regions (~ 0–3 kHz and 6–8 kHz), as predicted from the ensemble averages measured via MRI in Fig. 2 and ref. (*33*). Surprisingly, there is a notable increase in rate coefficient circa 5 kHz apparent in all systems, but most accentuated in the system with the slowest kinetics shown in Fig. 5I. It is possible that is ~5 kHz region indicates the mean autocorrelation time of free-tumbling monomers in solution, although concrete interpretation from these results alone is ambiguous.

***Reaction order parameters bridge kinetics and thermodynamics in heterogeneous processes***

Here, the frequency dispersion of the time-dependent depolymerization rate coefficients provide additional insight to the instantaneously calculated set of $k(t)$ reported in Fig. 2. From the set of $k(v, t)$ shown in Fig. 5G–I, it is possible to calculate frequency-dependent order parameters, $F(v)$, as the ratio of the initial to final $k(v, t)$, as demonstrated in Fig. 6A.(*32, 39, 40*) From this analysis, it becomes possible to attribute regions of relatively faster or slower reaction (i.e., temporally distinct behavior) to regions of the system spatially attributed to specific modes of diffusive behavior. These corresponding modes of diffusion can be understood to indicate regions of greater network confinement when their amplitudes over a given set of frequencies differs substantially from that of free water (which displays no effects of confinement and minimal effects of shear viscosity) and oil (with dipolar-coupled backbones, but no crosslinking or porous network confinement).

Additionally, by summing the individual frequency contributions that are spectrally resolved in Fig. 6A, a macroscopic order parameter(*32, 33, 41–43*) may be recovered as shown in Fig. 6B. The trend of increasing $F$ with variation of chaotropic to kosmotropic reaction media

qualitatively reflects the magnitude of changes in self-ordering that are necessary for the system for achieve thermodynamic equilibrium as the low-energy state associated with reaction completion. The most kosmotropic system considered here, $H_2SO_4$ (shown in red), begins in the most ordered state with the largest solvation shells, and therefore must undergo the greatest amount of change in terms of phase-restructuring to achieve uniformly mixed products. This process is diffusion-mediated and entropically driven. On the other hand, the most chaotropic system, HBr (shown in green), begins in the most randomized state that is closest to thermodynamic equilibrium, and thus presents the smallest order parameter. Interestingly, the reported trend in order parameter increasing together with kosmotropicity of the acid anion – a thermodynamic metric – is consistent with the observed trend in reaction rate coefficients. The correspondence between thermodynamic and kinetic factors is noteworthy and may play a role in the molecular dynamics of other systems influenced by slow kinetic processes whose operative timescales are similarly affected by thermodynamics and kinetics.

## Discussion

Efficient characterization strategies that illuminate both the structural architecture and dynamics of polymers during chemical transformations are urgently needed for improving global resource management. Such strategies will facilitate optimization and tuning of material properties that influence circular manufacturing processes. However, present literature lacks a thorough understanding of the coupling between transport and dynamics in macroscopically heterogeneous environments to the molecular-scale behaviors of water within confining media relevant to reactive elastomer networks. As a result, current treatments of molecular dynamics in polymer systems often fall short in capturing the complexity of transport processes, particularly those exhibiting time-variant, non-Euclidean boundary conditions. To bridge this gap, observation of frequency-dependent diffusion is powerful because it offers a direct link between structure and dynamics across scales, and is sensitive to both an aqueous medium and a polymer network in the experimental setup implemented here.

This study proposes an NMR-based method for characterizing the frequency-dependent diffusion of the various molecular moieties present in reactive elastomer networks swelled in aqueous media. When analyzed in the context of physical models parameterized with fractal mathematics, diffusion power spectra connect the microscopic, structural origins of differences in macroscopic deconstruction rates and large scale depolymerization outcomes. The proposed NMR-based MGSE method for measuring diffusion power spectra presents a promising avenue

11

for addressing the need for improved characterization strategies to guide a shift to a circular plastics economy, offering a wealth of chemical and mechanical information from a simple measurement that can be performed with readily customized benchtop NMR systems for *operando* studies.

Beyond calibration of the linear magnetic field gradient for calculation, we posit that normalization of diffusion power spectra via control samples is not valid in the same way that is for pulsed field gradient experiments calibrated to a standard, zero frequency value. This approach can potentially provide a prediction of the y-intercept in a diffusion spectrum, but the shape of the spectrum at nonzero frequencies is determined by a Lorentzian expression from the solution to the diffusion equation.(*12*) This not only accounts for zero frequency, or infinite time, translational motion, but also higher order vibrational movements determined by the density of states, degrees of freedom available to a system, and thus its crosslink density and degree of entanglement as shown in Fig. 1D. Additionally, correlated modes of mutual diffusion and non-Brownian motion may be included in the nonzero frequency part of the diffusion spectrum, thus mandating the use of an expression for mean squared displacement that can account for time dependence with fractionally scaled power laws.

By coupling experimental MGSE measurements of diffusion power spectra with physical models parameterized with fractal mathematics, we have attempted to demonstrate herein that the information accessible through this approach provides depth that can enhance insights from traditional methodologies. Furthermore, our findings underscore the potential of this technique to enhance the characterization and design of reactive polymers and complex materials, paving the way for advancements in circular materials economies and sustainable chemistry practices. This work not only contributes to fundamental understanding but also provides practical tools for engineering materials with tailored properties and behaviors, which we anticipate may serve to advance industrial applications.

**Materials and Methods**

***Experimental Design***

PDK elastomers were synthesized by ball-milling triketone monomer (1,10-bis(2-hydroxy-4,4-dimethyl-6oxocyclohex-1-en-1-yl)decane-1,10-dione) with tribranched amine-terminated polypropylene glycol cross-linkers T403, T3000, and T5000 (Huntsman), whose molar masses

are nominally 403, 3000, and 5000 g mol$^{-1}$, respectively.[44] A thorough description is provided in the SI Appendix. For swelling measurements, samples were immersed in an excess of $H_2O$ or $D_2O$ for a minimum of 1 week, to ensure that equilibrium had been achieved prior to measurement. Acids were prepared in 5 M concentration of HBr, HCl, and $H_2SO_4$ with chemicals were obtained from Sigma-Aldrich and used as received. Lewatit® VP OC 1065 was purchased from Sigma-Aldrich; the network molecules were evacuated prior to introduction of $H_2O$ or $D_2O$. Pluronic F-127 powder was purchased from Sigma-Aldrich; hydrogels were prepared at concentrations of 50% w/v with $H_2O$ and $D_2O$ by cooling below 10 °C to dissolve the powder, then heating above 10 °C to set the gel. Cooling and heating cycles were repeated 15-20 times over the course of 12 h until gels had achieved structural uniformity with no bubbles evident, appeared visually transparent, and irradiation with a collimated infrared laser beam did not result in scattered light.

NMR modulated gradient spin echo (MGSE) (*15, 17*) measurements were performed at room temperature with an NMR-MOUSE (Mobile Universal Surface Explorer) PM25 0.3 T unilateral magnet(*45, 46*) and a Magritek Kea II spectrometer at a $^1$H resonant frequency of 13.11 MHz. The number of π rf pulses in a Carr-Purcell-Meiboom-Gill pulse sequence (CPMG)(*47, 48*) were varied within a fixed total time to selectively detect the diffusive contribution to signal relaxation and not transverse relaxation, using Prospa v3.61 software from Magritek (Malvern, PA.). For all experiments, π/2 rf pulse lengths were 2.5 µs, the delay between π rf pulses was varied between 55 and 1100 µs in 20 incremental steps, and the repetition time for signal averaging was 2.4 s to sum either 128 or 4096 CPMG transient signals for the $H_2O$- and $D_2O$-based set of samples, respectively. To cancel artifacts arising from pulse imperfections, the initial π/2 rf pulse and the receiver were cycled between +x and −x phase while holding the π rf pulse phase constant at +y.

Imaging experiments were carried out with a Pure Devices 0.55 T Magspec magnet interfaced to Drive-L RF-100 and Gradient-600 amplifiers and an actively damped Q probe (Pure Devices GmbH, Germany), at a $^1$H resonant frequency of 24.36 MHz, and temperature controlled at 29 °C. Images were acquired using a standard spin echo pulse sequence (*49*) with an echo time of 5 ms and a repetition time of 5T1 = 1 s for the 5 M strong acids, to maximize signal from the aqueous acid and minimize signal from solid PDK with $R_2$ weighting. A 10 mm square field of view was chosen, corresponding to a 64x64 sampling grid with a slice thickness of 5 mm for axial images centered on polymer cylinders 6 mm in height and 8 mm in diameter placed in approximately 1 cc of acid. Zero-filling interpolated the square pixel resolution from 156.2 µm to 39.1 µm.

### Statistical Analysis

All simulations and data analysis were accomplished with MatLab (Mathworks, Natick, MA). The calculation of $D(\omega)$ from MGSE experiments was performed using a formula for echo attenuation as a function of gradient modulation frequency,

$$E(\tau, \omega_m) = \sum_i E_{0,i} e^{-\frac{\tau}{T_2} - \frac{8\gamma^2 G^2}{\pi^2 \omega_m^2} D_{zz,i}(\omega_m)\tau} \tag{5}$$

as previously derived via average Hamiltonian theory using a cumulant expansion to second order(*15, 17, 50*).

Measurements were collected in triplicate and error bars represent the statistical mean and standard deviation. Further mathematical derivation is provided in the SI Appendix.

### Acknowledgements

**Data Availability**: The data that support the findings of this study are available from the corresponding author upon reasonable request.

## References

1.    Ellen MacArthur Foundation, The New Plastics Economy – Rethinking the future of plastics. (2016).

2.    Ellen MacArthur Foundation, "The New Plastics Economy – Catalysing action" (2017).

3.    Ellen MacArthur Foundation, "The Global Commitment 2020 Progress Report" (2019).

4.    Y. Gefen, A. Aharony, S. Alexander, Anomalous Diffusion on Percolating Clusters. *Phys Rev Lett* **50**, 77–80 (1983).

5.    M.-O. Coppens, G. F. Froment, Diffusion and reaction in a fractal catalyst pore—I. Geometrical aspects. *Chem Eng Sci* **50**, 1013–1026 (1995).

6.    J. Crank, *The Mathematics of Diffusion* (Oxford University Press, Oxford , ed. 1, 1979).

7.    S. Wang, Z. Ma, H. Yao, Fractal diffusion model used for diffusion in porous material within limited volume of stiff container. *Chem Eng Sci* **64**, 1318–1325 (2009).

8.    B. O'Shaughnessy, I. Procaccia, Analytical Solutions for Diffusion on Fractal Objects. *Phys Rev Lett* **54**, 455–458 (1985).

9.    B. B. Mandelbrot, J. W. Van Ness, Fractional Brownian Motions, Fractional Noises and Applications. *SIAM Review* **10**, 422–437 (1968).

10.   C. Bousige, P. Levitz, B. Coasne, Bridging scales in disordered porous media by mapping molecular dynamics onto intermittent Brownian motion. *Nat Commun* **12**, 1043 (2021).

11.   J. Ślęzak, R. Metzler, Minimal model of diffusion with time changing Hurst exponent. *J Phys A Math Theor* **56**, 35LT01 (2023).

12.   M. Niknam, L.-S. Bouchard, Nuclear Induction Lineshape: Non-Markovian Diffusion with Boundaries. (2023).

13.   J. Stepišnik, P. T. Callaghan, The long time tail of molecular velocity correlation in a confined fluid: observation by modulated gradient spin-echo NMR. *Physica B Condens Matter* **292**, 296–301 (2000).

14.   J. Stepišnik, C. Mattea, S. Stapf, A. Mohorič, Molecular velocity auto-correlation of simple liquids observed by NMR MGSE method. *Eur Phys J B* **91**, 293 (2018).

15.   P. T. Callaghan, *Translational Dynamics and Magnetic Resonance* (Oxford University Press, 2011).

16.   D. A. McQuarrie, *Statistical Mechanics* (University Science Books, Sausalito, ed. 1, 2000).

17.   P. T. Callaghan, J. Stepišnik, Frequency-Domain Analysis of Spin Motion Using Modulated-Gradient NMR. *J Magn Reson A* **117**, 118–122 (1995).

18.   M. Hua, Z. Peng, R. Guha, X. Ruan, K. C. Ng, J. Demarteau, S. Haber, S. Fricke, J. Reimer, M. Salmeron, K. Persson, C. Wang, B. Helms, Mechanochemically Accelerated Deconstruction of Chemically Recyclable Plastics. *Sci Adv* **in press** (2024).

19. F. Vaca Chávez, K. Saalwächter, Time-Domain NMR Observation of Entangled Polymer Dynamics: Universal Behavior of Flexible Homopolymers and Applicability of the Tube Model. *Macromolecules* **44**, 1549–1559 (2011).

20. J. Tóth, A. L. Nagy, D. Papp, *Reaction Kinetics: Exercises, Programs and Theorems* (Springer New York, New York, NY, 2018).

21. T. X. Cai, N. H. Williamson, R. Ravin, P. J. Basser, Disentangling the Effects of Restriction and Exchange With Diffusion Exchange Spectroscopy. *Front Phys* **10** (2022).

22. K. Kulasinski, R. Guyer, D. Derome, J. Carmeliet, Water Diffusion in Amorphous Hydrophilic Systems: A Stop and Go Process. *Langmuir* **31**, 10843–10849 (2015).

23. D. Eager, A.-M. Pendrill, N. Reistad, Beyond velocity and acceleration: jerk, snap and higher derivatives. *Eur J Phys* **37**, 065008 (2016).

24. M. Visser, Jerk, snap and the cosmological equation of state. *Class Quantum Gravity* **21**, 2603–2615 (2004).

25. M. S. Green, Markoff Random Processes and the Statistical Mechanics of Time-Dependent Phenomena. II. Irreversible Processes in Fluids. *J Chem Phys* **22**, 398–413 (1954).

26. M. Doi, S. F. Edwards, *The Theory of Polymer Dynamics* (the Clarendon Press, Oxford University Press, New York, 1986).

27. W. R. Alesi, J. R. Kitchin, Evaluation of a Primary Amine-Functionalized Ion-Exchange Resin for $CO_2$ Capture. *Ind Eng Chem Res* **51**, 6907–6915 (2012).

28. J. F. Douglas, F. Horkay, Influence of solvent quality on the swelling and shear modulus of polymer gels chemically cross-linked in solution. *MRS Adv* **9**, 483–488 (2024).

29. A. Chremos, J. F. Douglas, P. J. Basser, F. Horkay, Molecular dynamics study of the swelling and osmotic properties of compact nanogel particles. *Soft Matter* **18**, 6278–6290 (2022).

30. J.-D. Bao, Time-Dependent Fractional Diffusion and Friction Functions for Anomalous Diffusion. *Front Phys* **9** (2021).

31. G. Parisi, N. Sourlas, Critical Behavior of Branched Polymers and the Lee-Yang Edge Singularity. *Phys Rev Lett* **46**, 871–874 (1981).

32. R. Kopelman, Fractal Reaction Kinetics. *Science (1979)* **241**, 1620–1626 (1988).

33. S. N. Fricke, S. Haber, M. Hua, M. Salgado, B. A. Helms, J. A. Reimer, Magnetic resonance insights into the heterogeneous, fractal-like kinetics of chemically recyclable polymers. *Sci Adv* **10** (2024).

34. B. B. Mandelbrot, Self-Affine Fractals and Fractal Dimension. *Phys Scr* **32**, 257–260 (1985).

35. A. Bunde, S. Havlin, Eds., *Fractals and Disordered Systems* (Springer Berlin Heidelberg, Berlin, Heidelberg, 1996).

36. K. Falconer, *Fractal Geometry* (John Wiley & Sons, Ltd, Chichester, UK, 2003).

37.   M. Kale, F. Butar Butar, Fractal analysis of time series and distribution properties of Hurst exponent. *J. Math. Sci. Math. Educ.* **5**, 8–19 (2011).

38.   S. Haber, J. Im, M. Hua, A. Epstein, S. Fricke, R. Giovine, H. Celik, K. Persson, B. Helms, J. Reimer, "Mechanisms Underpinning Heterogeneous Deconstruction of Circular Polymers: Insight from Magnetic Resonance Methodologies" (2024).

39.   S. V. Kalinin, D. L. Gorbachev, A. Yu. Borisevich, K. V. Tomashevitch, A. A. Vertegel, A. J. Markworth, Yu. D. Tretyakov, Evolution of fractal particles in systems with conserved order parameter. *Phys Rev E* **61**, 1189–1194 (2000).

40.   E. Salje, Kinetic rate laws as derived from order parameter theory I: Theoretical concepts. *Phys Chem Miner* **15**, 336–348 (1988).

41.   E. Salje, Kinetic rate laws as derived from order parameter theory I: Theoretical concepts. *Phys Chem Miner* **15**, 336–348 (1988).

42.   S. V. Kalinin, D. L. Gorbachev, K. V. Tomashevitch, A. Yu. Borisevich, A. A. Vertegel, A. J. Markworth, Yu. D. Tretyakov, Evolution of Fractal Particles in Systems with Conserved Order Parameter. *MRS Proceedings* **538**, 151 (1998).

43.   M. McCormick, J. A. Reimer, NMR Studies of Structural Phase Transitions in Random Copolymers. *Macromolecules* **36**, 477–485 (2003).

44.   P. R. Christensen, A. M. Scheuermann, K. E. Loeffler, B. A. Helms, Closed-loop recycling of plastics enabled by dynamic covalent diketoenamine bonds. *Nat Chem* **11**, 442–448 (2019).

45.   G. Eidmann, R. Savelsberg, P. Blümler, B. Blümich, The NMR MOUSE, a Mobile Universal Surface Explorer. *J Magn Reson A* **122**, 104–109 (1996).

46.   B. Blümich, J. Anders, When the MOUSE leaves the house. *Magnetic Resonance* **2**, 149–160 (2021).

47.   H. Y. Carr, E. M. Purcell, Effects of Diffusion on Free Precession in Nuclear Magnetic Resonance Experiments. *Physical Review* **94**, 630–638 (1954).

48.   S. Meiboom, D. Gill, Modified Spin-Echo Method for Measuring Nuclear Relaxation Times. *Review of Scientific Instruments* **29**, 688–691 (1958).

49.   B. Blümich, *NMR Imaging of Materials* (Clarendon Press, 2003).

50.   J. Stepišnik, Validity limits of Gaussian approximation in cumulant expansion for diffusion attenuation of spin echo. *Physica B Condens Matter* **270**, 110–117 (1999).

**Figures and Tables**
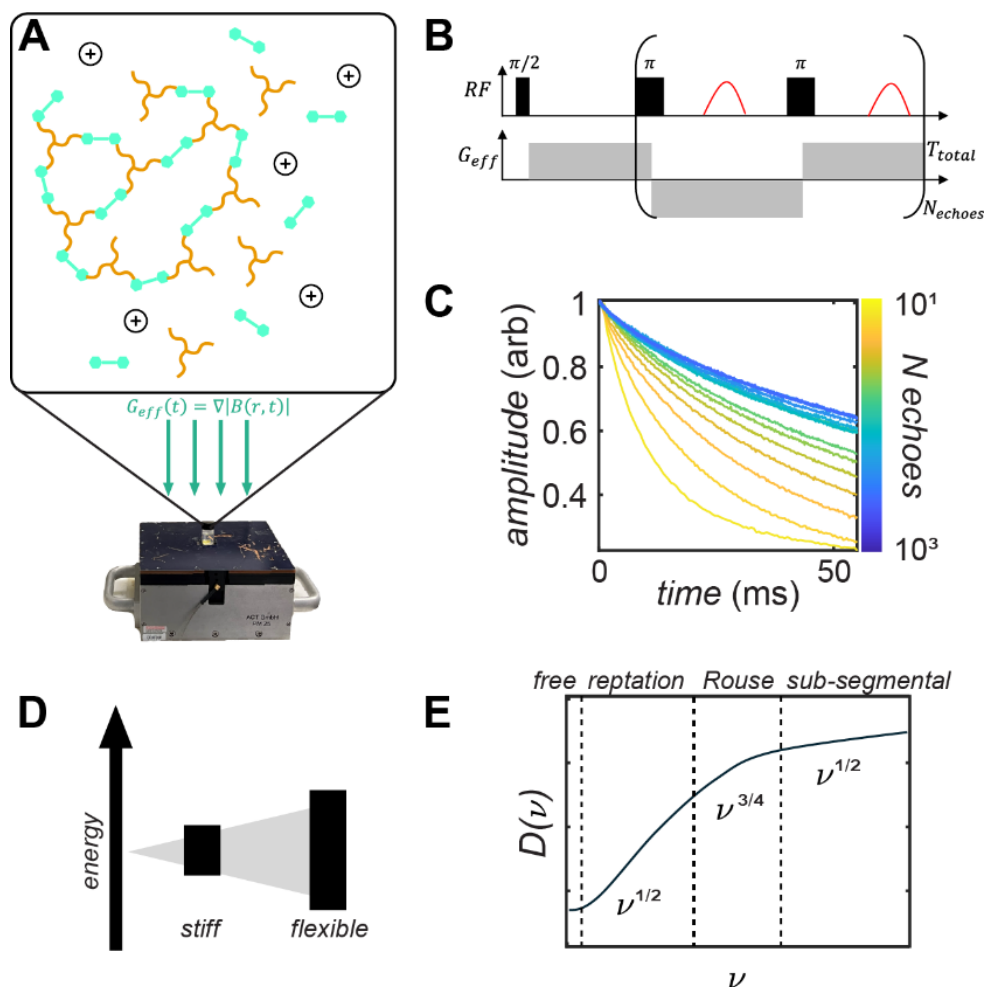


**Figure 1. A graphical depiction of polymer transport, diffusion, and reaction as measured with an MGSE experiment using benchtop NMR.** Figure 1A shows a polymer sample atop a 0.3 T PM25 NMR-MOUSE unilateral magnet with a static linear gradient, $G_{eff}$, of 7 T m$^{-1}$. Figure 1B shows the MGSE pulse sequence, wherein the number of $\pi$ RF pulses in an echo train is varied within a fixed total time, $T_{total}$, resulting in a set of echo time decays as shown in Fig. 1C, with exemplary data for a micellar block copolymer gel made of 50% w/v Pluronic F-127 in H$_2$O. The energy level diagram in Fig. 1D shows the effect of entanglement on the density of states. In turn, this affects the dynamic regimes accessed by a polymer system, which are depicted according to the polymer tube model in Fig. 1E.
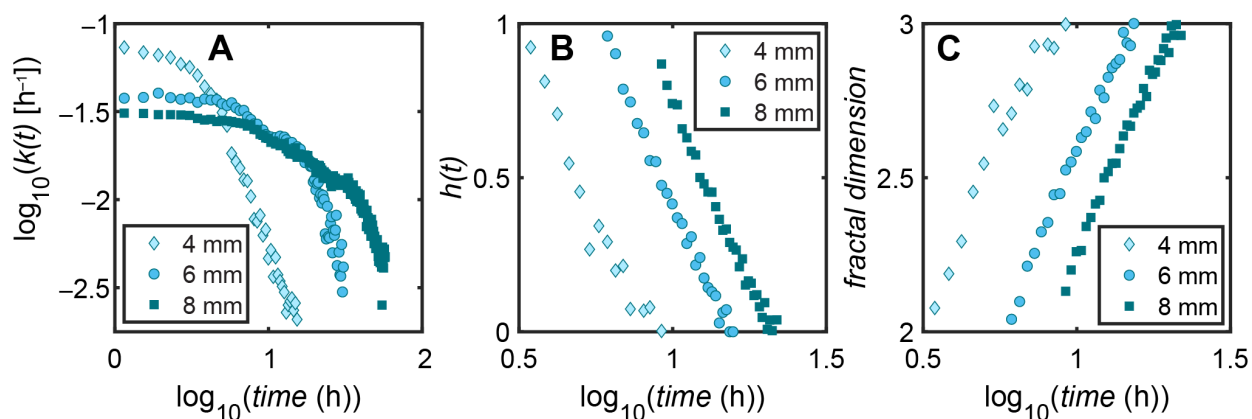
**Figure 2. A demonstration of the scale variance of depolymerization reaction kinetics.** The comparative time-dependent rates of PDK-T5000 cylinders of three different diameters deconstructing in 5 M $H_2SO_4$, as calculated from *operando* MR images. From the set of $k(t)$ in Fig. 2A, the time-dependent Hurst exponents, $h(t)$, and the fractal dimension are calculated in Figs. 2B and 2C as $\frac{\partial k}{\partial t}$ and $3 - h$, respectively.

19
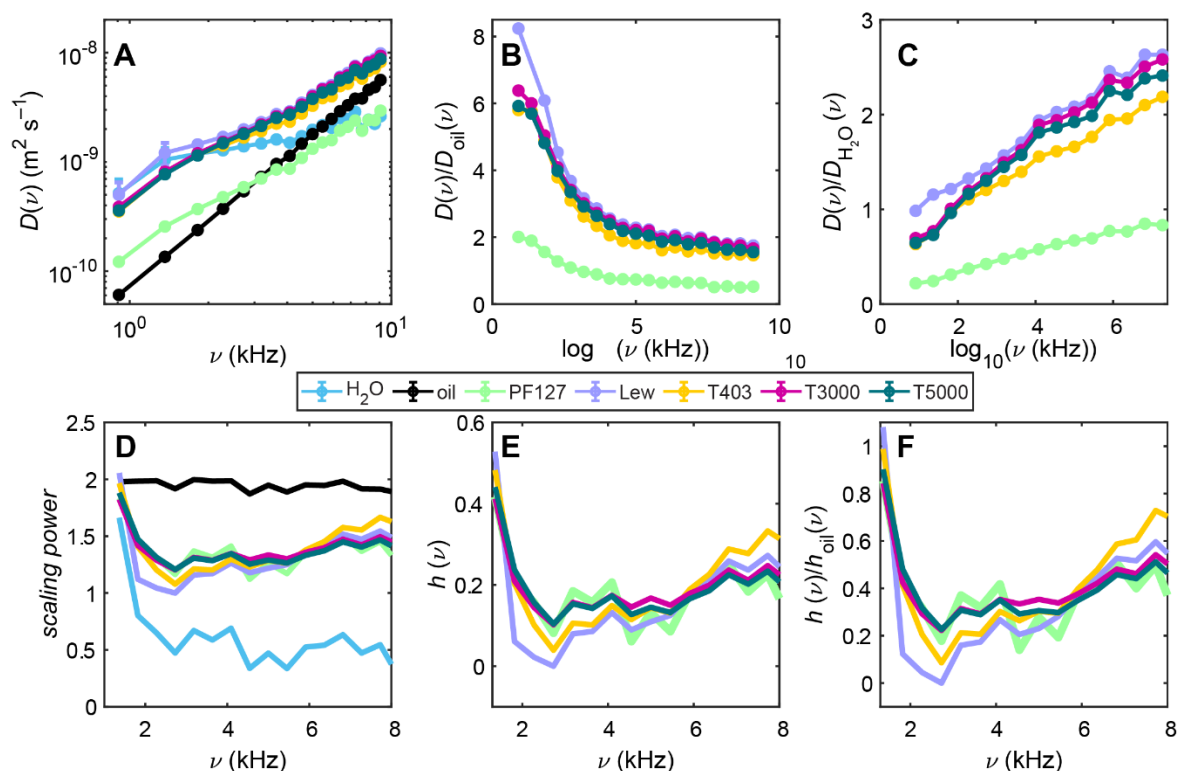
**Figure 3. Diffusion power spectra report the Hurst exponent of water confined in various polymer environments with non-evolving pore structures.** (A) $D(\nu)$ for water confined in a representative selection of polymers: network PDKs of different crosslinking density (PDK-T403, PDK-T3000, PDK-T5000), and Lewatit, compared to $D(\nu)$ of an aqueous 50% w/v Pluronic F-127 gel. Figure 3B shows these spectra relative to the diffusion spectrum of oil, a representative dipolar-coupled network without crosslinking. Figure 3C shows these spectra relative to the diffusion spectrum of freely diffusing water. The scaling powers of the diffusion spectra reported in Fig. 3D connect to the frequency-resolved Hurst exponents, $h(\nu)$, shown relative to the frequency-resolved Hurst exponent of oil in Fig. 3E.
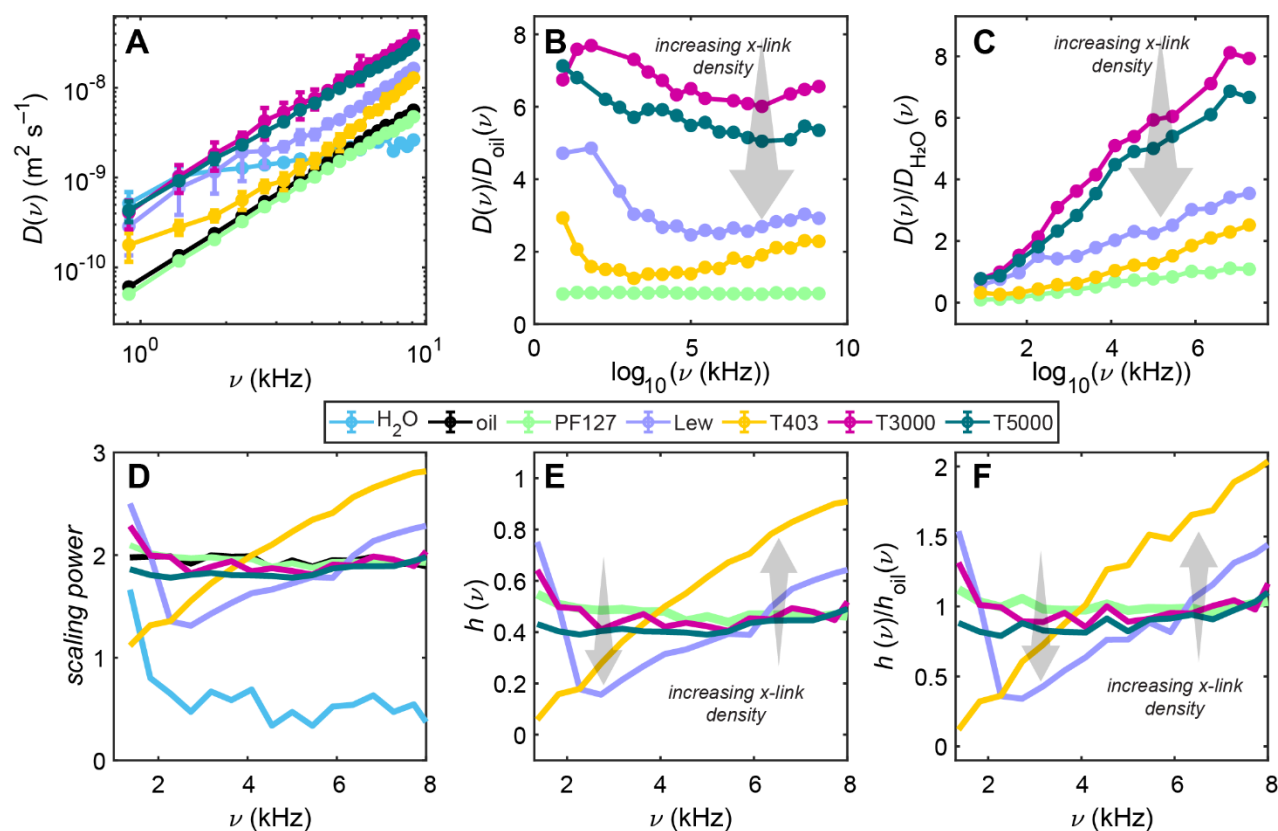
**Figure 4. Diffusion power spectra yield the Hurst exponent of polymer motional modes with non-evolving pore structures.** (A) $D(\nu)$ for a representative selection of polymers swelled with $D_2O$: network PDKs of three crosslink densities (PDK-T403, PDK-T3000, PDK-T5000) and Lewatit, compared to $D(\nu)$ of a deuterated aqueous 50% w/v Pluronic F-127 gel. Figure 4B shows these spectra relative to the diffusion spectrum of oil, a representative dipolar-coupled network without crosslinking. Figure 4C shows these spectra relative to the diffusion spectrum of freely diffusing water. The scaling powers of the diffusion spectra reported in Fig. 4D connect to the frequency-resolved Hurst exponents, $h(\nu)$, shown relative to the frequency-resolved Hurst exponent of oil in Fig. 4E.
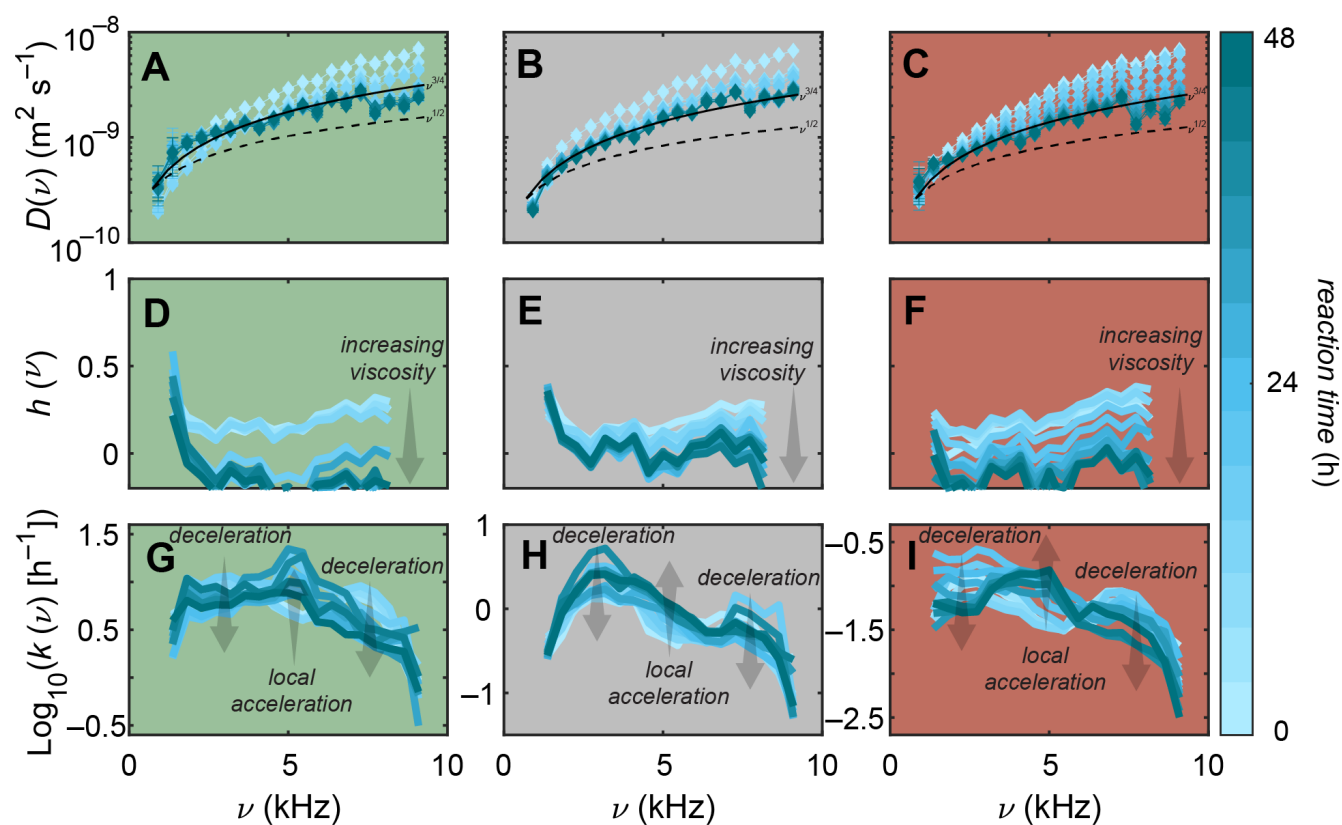
**Figure 5. Overlaid diffusion power spectra for deconstructing PDK-T5000 cylinders 6 mm in diameter and 5 mm in height in 5 M HBr, HCl, and H$_2$SO$_4$ (A-C) yield time- and frequency-resolved Hurst exponents which predict rate coefficients.** From numerically integrating $h(\nu, t)$ with respect to time, as plotted in Fig. 5D–F and calculated from the Fig. 5A–C, it is possible to predict $k(\nu, t)$. As the fastest-depolymerizing system considered here, the PDK-T5000 reacting in HBr (green backdrop; left column) reaches completion of reaction first, which is clear in Fig. 5D as the sudden drop in $h(\nu, t)$ at 24 h toward zero mean. The slowest-depolymerizing system here is PDK-T5000 reacting in H$_2$SO$_4$, plotted with a red backdrop in the right-most column. PDK-T5000 deconstructing in HCl presents a reaction of intermediate rate, plotted with grey backdrop in the center column.

22
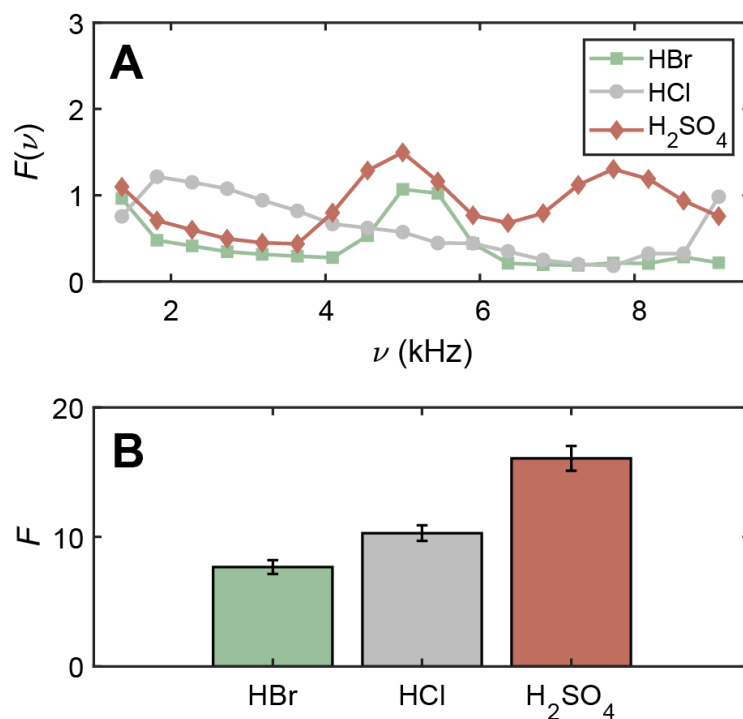
**Figure 6. Frequency dispersion of reaction order parameters.** (A) compares the frequency-dependent order parameters for PDK-T5000 depolymerization in 5 M HBr, HCl, and $H_2SO_4$, calculated from the ratio of the initial to final $k(v, t)$ plotted in Fig. 5G-I. By summing all the individual frequency contributions to $F(v)$, it is possible to calculate a macroscopic order parameter, $F$, independent of frequency, to contrast the differing reaction systems in (B).